Improving OFDR Distributed Fiber Sensing by Fibers with Enhanced Rayleigh Backscattering and Image Processing

Qirui Wang, Kehao Zhao, Mudabbir Badar, Xinruo Yi, Ping Lu, *Member*, *IEEE*, Michael Buric, Zhi-Hong Mao, *Senior Member*, *IEEE*, and Kevin P. Chen

***Abstract*—This paper investigates using optical fibers with enhanced backscattering profiles to improve distributed fiber sensor performance and reduce instrumentation costs. Using a femtosecond laser direct writing technique, the Rayleigh backscattering profile of a standard telecom fiber was enhanced by more than 40 dB to improve the signal-to-noise ratio for optical frequency domain reflectometry (OFDR). The enhanced backscattering signals enable effective distributed strain measurements using a low-cost tunable laser. Median filtering is applied to denoise cross-correlation results to further improve measurement outcomes. Results presented in this paper show that a tunable laser with a 1-nm tuning range, which is far less than the tuning range used in commercial OFDR interrogators, can perform effective distributed strain measurements using sensing fibers with enhanced backscattering profiles. The sensing fiber with over 40-dB backscattering enhancement achieved 4.8-cm spatial resolution in strain measurements with a root mean square accuracy of less than 2.70 με when 10 με to 50 με were exerted to the sensing fiber. Results presented in this paper reveal both the potential and limitations of sensing fibers with enhanced backscattering for OFDR-based distributed fiber sensors.**

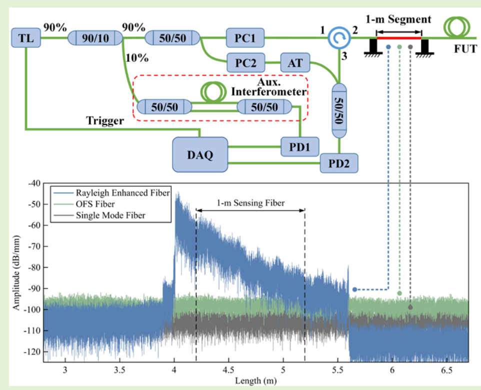

***Index Terms*—Backscattering, image processing, optical frequency domain reflectometry, strain sensing**

I. Introduction

DISTRIBUTED fiber sensors that exploit Rayleigh backscattering processes in unmodified standard telecommunication fibers have been successful in performing high spatial resolution measurements of physical parameters such as temperature, strain, vibration, and others [1]–[4]. By using the coherent backscattered light produced by standard telecom optical fibers, commercial optical frequency domain reflectometers (OFDR) have reported 1-cm spatial resolution continuous measurement of temperature and strain using standard telecom fibers to achieve up to 0.1℃ temperature sensing resolution and 1-με strain sensing resolution [5]. Optical time domain reflectometry (OTDR) relying on Rayleigh backscattering in unmodified fibers has also been used to perform distributed acoustic sensing over fiber lengths greater than 10 km [6]. However, unmodified standard fibers produce extremely weak Rayleigh backscattering signals as they are designed for ultra-low-loss telecom applications, which results in a poor signal-to-noise ratio (SNR) for Rayleigh sensing applications, and severely compromises the overall performance of both OFDR and OTDR systems [7].

To overcome the weak backscattering issue, the OFDR scheme requires a high-performance tunable laser (TL) with a wide wavelength tunning range to collect a large number of data points to improve SNRs. For the OTDR scheme, the weak backscattering signals also demand highly sensitive photodetectors with sufficiently low dark noise and high bandwidth to achieve the desired spatial resolution and performance. Both lead to high interrogation instrument costs that reduce applicability of the distributed sensor technology.

The other approach to improve SNR is to use specialized sensing fibers where backscattered signals are artificially enhanced through laser irradiation. In this approach, both ultraviolet (UV) lasers [8] and femtosecond (fs) ultrafast lasers [9] have been used to enhance the backscattering signals in optical fibers to achieve a better SNR. It has been shown that a fiber with enhanced backscattering can improve strain and temperature measurement resolution [10]. Recently, nanoparticle-doped fibers are also studied by researchers to

Manuscript received Month xx, 2xxx; revised Month xx, xxxx; accepted Month x, xxxx. This work was supported in part by the Department of Energy through Office of Nuclear Energy's grants DE-NE0008686 and DE-NE0008994, and in part by the Department of Energy, National Energy Technology Laboratory, an agency of the United States Government, through a support contract with Leidos Research Support Team (LRST). (*Corresponding author: Kevin P. Chen.*)

Qirui Wang, Kehao Zhao, Xinruo Yi, Zhi-Hong Mao, and Kevin P. Chen are with the Department of Electrical and Computer Engineering, University of Pittsburgh, Pittsburgh, PA 15261 USA (e-mail: qiw53@pitt.edu; kez23@pitt.edu; xiy86@pitt.edu; zhm4@pitt.edu; pec9@pitt.edu).

Mudabbir Badar was with the National Energy Technology Laboratory, Pittsburgh, PA 15236 USA, at the time of conception of the paper (e-mail: mudabbir.badar@netl.doe.gov).

Ping Lu is with OFS Fitel, LLC, Avon, CT 06001 USA (e-mail: plu@ofsoptics.com).

Michael Buric is with the National Energy Technology Laboratory, Morgantown, WV 26505 USA (e-mail: michael.buric@netl.doe.gov).

obtain a high SNR and high-gain backscattering profiles in various distributed sensing applications [11]–[15]. They show promising properties for distributed and multiplexing sensing.

However, the other less-explored aspect of using specialized or enhanced sensing fibers is the potential to develop distributed fiber sensor interrogators using low-cost laser sources and detectors. If a fiber enhanced backscattering is available, then a much smaller number of data points are needed to perform distributed sensing measurements. As a result, a TL with a much narrower wavelength tuning range could be sufficient for an OFDR system. This paper explores this possibility.

In this paper, sensing fibers with backscattering profiles enhanced by either UV or fs laser are used to perform distributed strain sensing. By limiting the wavelength tuning range of the OFDR's TL to 1 nm, this paper studies how the enhancement of backscattering signals influences the overall measurement performance for distributed fiber sensors. Through systematical studies of the OFDR measurement scheme using a fiber with 20-40 dB backscattering enhancements, this paper provides a quantitative evaluation on how SNR enhancement could impact the sensor performance and the cost of interrogation systems.

II. Experimental Setup and Principle

Fig. 1 shows the schematic of an OFDR distributed fiber sensing interrogation system. A TL (Furukawa Fitel FRL15DCWD) was used as an optical source. The tuning range of the laser was limited to 1 nm. The optical signal output from the TL is split by a 90/10 optical coupler into two arms. The low-power arm is connected to an auxiliary Mach-Zehnder interferometer to correct nonlinear tuning. The high-power arm feeds two polarization controllers (PC's) that comprise a main interferometer along with an attenuator (AT) and a fiber under test (FUT). There is a 1-m segment of the FUT mounted between two translation stages (Newport 423 series) for distributed strain sensing. The original distance between two stages is 1 m. And a Vernier micrometer (Newport SM-25) with 1-μm sensitivity drives a stage to exert strain on the sensing fiber. Using multiple setups, different levels of strain can be applied to different sections of the fiber. Two photodetectors (PD's, Menlo Systems FPD510-FC-NIR) and a data acquisition (DAQ, AlazarTech ATS9440) device are utilized to acquire interference signals from both auxiliary and main interferometers.

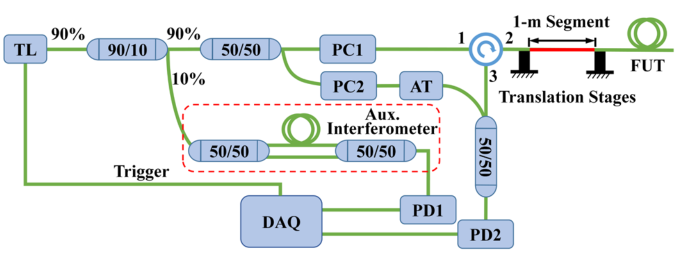

Fig. 1. Schematic of the OFDR strain sensing system for testing enhanced sensing fibers.

A. Sensing Fiber

To explore the performance of the OFDR interrogation scheme with enhanced sensing fibers, three types of fibers were used for experiments. These included standard unmodified telecom fibers (Corning SMF-28e+) which have been commonly used for distributed sensing, fibers enhanced via ultrafast laser irradiation, and commercially available UV-exposed enhanced fiber (OFS AcoustiSens Wideband). To further improve SNR, a fs laser direct writing technique was used to enhance Rayleigh backscattering on the standard telecom fiber. The detailed fabrication method for this fiber can be found in [16] and briefly described here.

During the fabrication, a 100× aberration-corrected microscope objective (NA = 0.75) was used to focus the beam. The 800-nm laser was focused into the center of the optical fiber core enabled by a set of high-precision motorized stages (Aerotech ABL2000). The dimension of the modification area was around 2 μm × 2 μm × 6 μm. To achieve continuous femtosecond laser inscription, the fiber was translated using a customized reel-to-reel setup at a constant speed of 1 mm/s. Laser beam was linearly polarized, with its direction of polarization perpendicular to the direction of fiber translation. The backscattering behavior of the fiber sample was monitored in real-time using a commercial optical backscatter reflectometer (LUNA Innovation OBR 4600).

Systematical laser fabrication studies have been carried out to study propagation loss and Rayleigh backscattering enhancements vs. laser parameters used to inscribe sensing fibers [16]. The location of the laser irradiated area and the pulse energy are two main factors impacting the propagation loss and scattering enhancement. The scattering enhancement is strongest when the irradiated area is located in the center of the fiber core. When the irradiation deviates to the interface of the core and cladding, the loss increases and the enhancement decreases significantly. In terms of the pulse energy, no modification occurs if it is under the threshold of ~10 mW. Higher pulse energy would lead to stronger scattering enhancement and propagation loss. The laser processing parameters (80-nJ pulse energy, 270-fs pulse width, 250-kHz repetition rate) were intentionally chosen to produce Type-II modification with high loss to study the impact of backscattering signal strength on the overall performance of OFDR measurements.

The laser direct writing process generated an over 50-dB enhancement of the Rayleigh backscattering signal in a ~1.6-m FUT segment as shown in Fig. 2. A 1-m section of the enhanced portion (from 4.2 m to 5.2 m) was mounted between two translation stages using adhesive, while the Rayleigh backscattering was enhanced between 20 dB (at 5.2 m) to 40 dB (at 4.2 m).

For the UV enhanced fiber (OFS), the Rayleigh backscattering profile has been enhanced by ~10 dB in production through random fiber Bragg grating induced UV laser irradiation, which results in a smooth Rayleigh backscattering profile over fiber length as shown in Fig. 2.

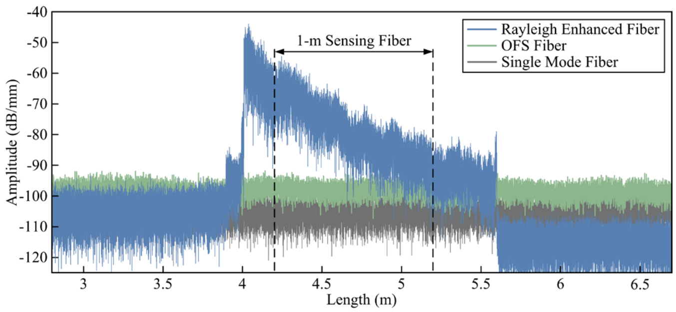

Fig. 2. Rayleigh backscattering profiles of Rayleigh enhanced sensing fiber, OFS AcoustiSens fiber, and standard single mode fiber.

B. Nonlinear Sweep Correction

In OFDR applications, a completely linear TL wavelength sweep-tuning is desired, but is often hard to achieve in practice. The electric field of the TL can be expressed as

$$E_0(t) = E_0 \exp[j\varphi(t)] \tag{1}$$

where E_0 is the amplitude and $\varphi(t)$ is the phase, which varies with time. If the amplitude is a constant, the instantaneous optical frequency of the TL can be written as follows:

$$v(t) = \frac{1}{2\pi}\frac{d\varphi(t)}{dt} \tag{2}$$

The optical frequency sweep rate of the TL is described by

$$k(t) = \frac{dv(t)}{dt} \tag{3}$$

Thus, the frequency sweep rate would be constant if the instantaneous optical frequency $v(t)$ is linearly tuned.

From Fig. 1 it can be seen that the beat signal generated by the auxiliary interferometer would be detected by PD1. Its intensity can be expressed as [17]

$$I(t) = I_0 \cos[\varphi(t) - \varphi(t-\tau_A)] \tag{4}$$

where I_0 is the amplitude and τ_A is the time delay caused by the optical path difference in the auxiliary interferometer. Next, a Taylor expansion is performed on the phase term, and since higher-order terms of the phase's Taylor expansion are trivial and neglected [18], (4) can be rewritten as

$$I(t) = I_0 \cos[\tau_A \frac{d\varphi(t)}{dt}] = I_0 \cos[2\pi\tau_A v(t)] \tag{5}$$

The phase of the auxiliary interferometer signal can be obtained by taking the Hilbert transform as below:

$$\Phi(t) = 2\pi\tau_A v(t) = \arctan\frac{H[I(t)]}{I(t)} \tag{6}$$

Finally, the instantaneous optical frequency is given by

$$v(t) = \frac{1}{2\pi\tau_A}\arctan\frac{H[I(t)]}{I(t)} \tag{7}$$

Therefore, the optical frequency sweep can be linearized based on the frequency information extracted from the auxiliary interferometer by using resampling algorithms [4].

C. Cross-Correlation Processing

Raw data collected through the main interferometer at different strain levels are corrected to linearize the optical frequency as it is swept. One of the resampled traces can be treated as reference data while the rest are treated as measurement data. Cross correlation is then performed between the reference and measured traces to calculate the strain using the following procedure:

1) Fast Fourier transforms (FFT) are applied on the reference and the measurement traces so that data are transformed from the optical frequency domain into the spatial domain.
2) Both the reference and the measurement spectra are equally divided into multiple windows. Each window represents a small segment of the FUT and the window size reflects the spatial resolution of the OFDR sensing system.
3) Two windows having the same spatial position index are extracted from two spectra separately. They are zero padded and then converted back to the optical frequency domain via an inverse FFT (IFFT) to calculate corresponding Rayleigh backscattering spectra (RBS) [19].
4) Cross-correlation between the reference and the measurement RBS is calculated to determine the RBS shift, which indicates the sensing parameter's variation, i.e., strain change, at the current position index [20].
5) Steps 3 and 4 are repeated for all window indices to obtain the strain change all along the length or at all spatial position indices.

For Step 2, assuming the optical frequency tuning range is ΔF and the tuning rate is k, the tuning time is

$$t = \frac{\Delta F}{k} \tag{8}$$

In this paper, since the wavelength sweep range is only 1 nm, the frequency tuning range ΔF would be 125 GHz. Given the sampling rate f_s, the total number of data collected by the DAQ module within a tuning period is

$$M = f_s t \tag{9}$$

If the length of FUT is L, the propagation delay τ can be expressed as

$$\tau = \frac{2nL}{c} \tag{10}$$

where c is the speed of light in a vacuum and n is the refractive index of the medium (fused silica glass). The number of data points corresponding to the FUT in the spatial domain is:

$$N = \frac{k\tau}{f_s}M = kt\tau \tag{11}$$

Therefore, the two-point resolution can be written as

$$\Delta z = \frac{L}{N} = \frac{c}{2n\Delta F} \tag{12}$$

Assuming the number of data points within each window in Step 2 is W, the spatial resolution of an OFDR system can be written as

$$R = W\Delta z = W\frac{c}{2n\Delta F} \tag{13}$$

As the wavelength sweep range decreases, the frequency tuning range goes down, and the two-point resolution goes up. Although less data would be needed in a sliding-window scheme to implement cross-correlations at a narrower sweep range, the value of the system spatial resolution would have to be increased to generate reasonable sensing results. For instance, a given commercial OBR 4600 has a wavelength tuning range of 80 nm. The optical frequency tuning range is 10,000 GHz and the two-point resolution is as small as 10 µm. The OBR 4600 uses 1,000 data points in a sliding window to achieve a 10-mm spatial resolution as reported in its datasheet

[5]. To contrast, the system reported here utilizes a 1-nm tuning range and exhibits a two-point resolution of 800 µm. By using the fiber with Rayleigh backscattering enhancements, 110 data points are required for the sliding window scheme. However, the system spatial resolution is 88 mm, which is nearly nine times worse than the spatial resolution of the OBR 4600 due to the sweep range limit.

D. Median Filtering

To improve performance of distributed fiber sensors, various imaging processing algorithms have been applied to reduce impacts of noise in measurement data harnessed by Raman and Brillouin sensors [21], [22]. To utilize these image denoising algorithms, spatial-domain data sets harnessed by distributed fiber sensors are segmented and computed to obtain cross-correlation results at all lags for each segment. And the results at all segments can form a two-dimensional image. An example is shown in Fig. 3(a). The OFDR measurements in the spatial domain produced by a TL with 1-nm wavelength tuning across a 1.6-m long sensing fiber are divided into 15 segments. These segments are labeled as spatial position index (SPI) 1-15 as shown in Fig. 3(a). Each pixel along the vertical axis represents the spatial resolution of the OFDR system. At a certain SPI, the row indicates cross-correlation results at a series of successive lags for that segment. And the normalized value of the cross-correlation result is expressed in color. The needed cross-correlation shift at each SPI, resulting from external strain or temperature changes, can be determined by the horizontal lag of the pixel which has the greatest cross-correlation value in that row. The cross-correlation shift is proportional to the RBS shift as well as to the strain change. By extracting cross-correlation shifts at all SPI, another image representing strain changes along the FUT can be acquired as shown in Fig. 3(b).

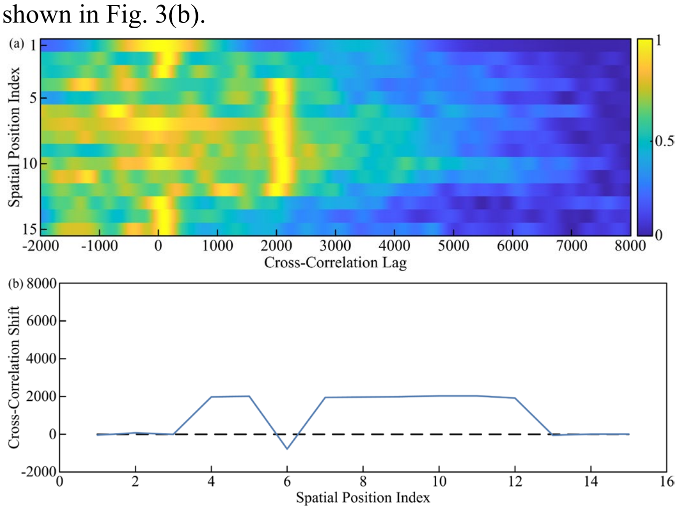

Fig. 3. Cross-correlation results acquired via the OFDR system: (a) a two-dimensional image containing complete cross-correlation results along the FUT; (b) strain change detection results by using cross-correlation shifts in each row.

Corresponding to the short 1-nm sweep range of the TL, the two-point resolution of an OFDR system would be much larger than a typical commercial system with a much larger wavelength sweep range (e.g., 40-80 nm). In order to maintain a satisfactory spatial resolution, the number of data points within a window has to be reduced, which would cause the deterioration of cross-correlation results and produce erroneous strain measurement results. As shown in Fig. 3(a), a sudden spike was produced by the cross-correlation computations at SPI 6, which results in a spectral shift value around -800. The conventional cross-correlation algorithm converts this shift value to the strain incurred at the location by mistake, which will severely impact accuracies of the OFDR. In general, as the size of the sliding window decreases, more mis-characterized non-maximal pixels would appear and the OFDR system would become less accurate.

In order to remove erroneous cross-correlation calculations occurred using a laser with a short sweep range, median filtering algorithm [23] can be applied to denoise the two-dimensional images (Fig. 3(a)) and suppress pixel values which are unrepresentative of their surroundings. The kernel size of the median filter is set to be 3×1 to eliminate abrupt strain changes along the vertical orientation. Additionally, in traditional processing when a spectrum is divided into windows in the spatial domain, those windows are connected end to end, which means the step size between two adjacent windows is exactly the size of one window. However, this operation would result in the deterioration of spatial resolution [24]. Therefore, an overlapping window division method was used in this work and the step size can be shorter than a window size. By making a tradeoff between the spatial resolution and the computational load, the step size is set to be 1/10 of the window size.

III. Results and Discussion

Operating parameters for the OFDR strain sensing system described here are summarized in Table I.

TABLE I
OFDR Sensing System Parameters

Parameter	Value
Wavelength sweep range	1549.118-1550.121 nm
Frequency sweep range	125.219 GHz
Two-point resolution	0.8 mm
TL tuning rate	100.3 nm/s
DAQ sampling rate	10 MHz

To validate the distributed strain sensing capabilities of the OFDR system with a short sweep range, the Rayleigh enhanced sensing fiber, the OFS fiber, and a standard telecom single mode fiber were all mounted on a pair of translation stages to induce strain. The main interferometer's signal without any strain applied was used as the reference signal after nonlinear wavelength tuning correction. Different levels of strain from 10 µε through 50 µε with a step size of 10 µε were exerted on the 1-m sensing fiber segment. By following the processing procedures discussed above, the main interferometer's signal at each strain level was sampled, corrected, and finally cross-correlated with the reference signal respectively to calculate corresponding strain changes. The same interrogation settings and calculations were applied for all three test fibers. Fig. 4 shows the distributed strain sensing results without applying denoising for the Rayleigh enhanced fiber, the OFS fiber, and the standard telecom fiber, respectively. The non-overlapping sliding windows were applied to perform cross-correlation calculations. Each sliding window has 110 data points and the spatial resolution is 88 mm.

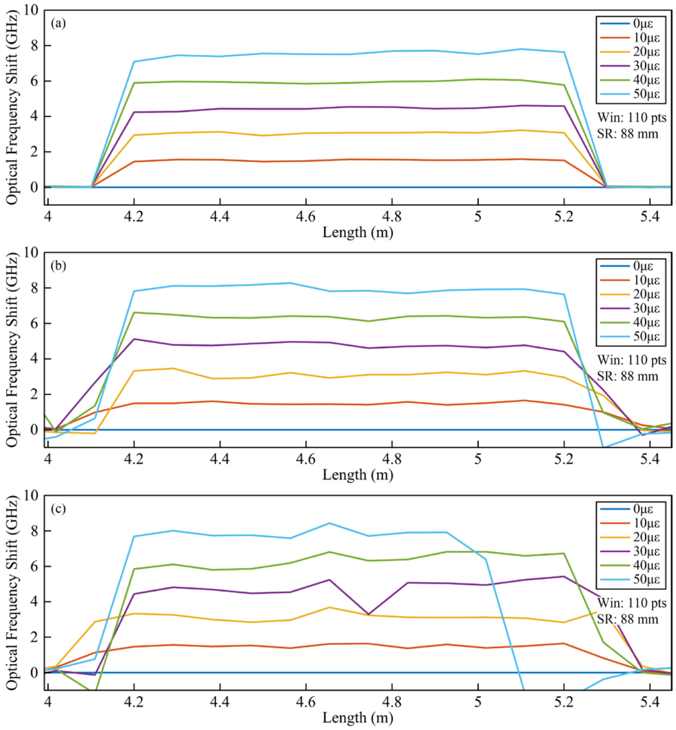

Fig. 4. Distributed strain sensing results with a window of 110 data points and a spatial resolution of 88 mm: (a) Rayleigh enhanced sensing fiber; (b) OFS fiber; (c) standard single mode fiber.

As can be seen in Fig. 4(a), there are 5 distinct strain levels measured along the 1-m Rayleigh enhanced sensing segment. The Rayleigh enhanced fiber provides the best strain sensing performance among all test fibers. In comparison, Fig. 4(b) displays non-realistic variations in the detected strain at both ends of the 1-m OFS sensing fiber segment as a result of the limited strain accuracy with this limited interrogator sweep range. Fig. 4(c) presents sensing results for the standard telecom single mode fiber. The poor SNR as a result of the weak Rayleigh backscattering signal yields erroneous cross-correlations. Results for the OFS fiber and standard telecom fiber can be improved by increasing the size of the sliding window at the expense of a poor spatial resolution. The OFS fiber and the single mode fiber can provide satisfactory sensing results from 10 με through 50 με with a sliding window of 170 data points (136 mm) and 200 data points (160 mm) respectively. Results presented in Fig. 4 illustrate the improvement offered by the direct laser writing technique for use with low-cost interrogation systems powered by a laser with narrower wavelength tuning ranges.

To further study the strain sensing performance of these optical fibers, the root mean square errors (RMSE) for optical frequency shifts at each strain level for both standard fiber and enhanced fibers are computed and compared in Fig. 5(a). The fs-enhanced fiber, which exhibits a drastic increase in backscattering signal strength of 20-40 dB, produces the best results with RMSE less than 1.23 με. For the UV-enhanced OFS fiber, the much more conservative 10-dB improvement in backscattering signal provides a more limited improvement over the standard fiber results. RMSE values for the OFS fiber scale roughly linearly with strain levels. At 50 με, the measured RMSE is 4.18 με, which is more than five times better than that of standard fibers. However, it is more than three times worse than that of the fs-enhanced fiber. Fig. 5(b) plots the average optical frequency shift vs. the strain exerted on the fibers. All fibers exhibit linear relationships between the average optical frequency shift as a function of strain change. Strain sensitivity coefficients (the slope of lines in Fig. 5(b)) for the fs-enhanced fiber, the UV-enhanced fiber, and the standard fiber are 0.149 GHz/με, 0.160 GHz/με, and 0.135 GHz/με respectively. These values are consistent with the reported strain sensitivity coefficient 0.15 GHz/με [25], which confirms the validity of our measurements.

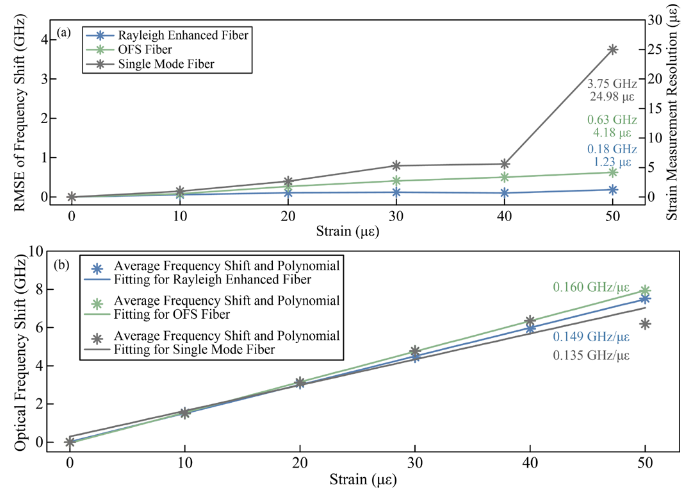

Fig. 5. Processing of strain sensing results for all three test fibers with 88-mm spatial resolution: (a) RMSE of optical frequency shifts and strain measurement resolutions at five strain levels; (b) linear relationships between exerted strain and average optical frequency shift.

Fig. 6 shows the effect of the size of the sliding window on the quality of strain sensing measurements using the Rayleigh enhanced fiber as the window was narrowed from 110 data points down to 60 points, which corresponds to a spatial resolution ranging from 88 mm to 48 mm. Apparently, the Rayleigh enhanced fiber is unable to perform effective strain sensing measurements with such a small window size and a reduced spatial resolution.

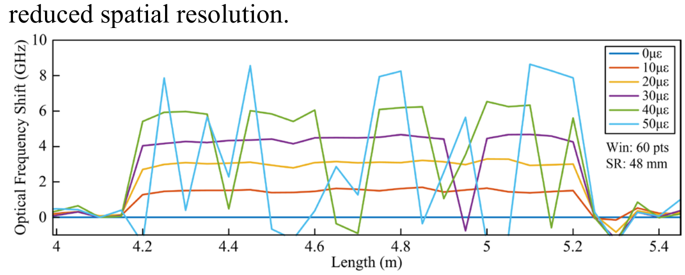

Fig. 6. Distributed strain sensing results with a window of 60 data points and a spatial resolution of 48 mm based on the Rayleigh enhanced sensing fiber.

In order to improve the spatial resolution of the OFDR system for smaller window sizes while ensuring sensing effectiveness, the overlapping window division method and median filtering were applied to the data. Similarly, five levels of strain were exerted on the sensing segments sequentially. The sliding window had 60 data points with a step size of 6 data points, which corresponds to a spatial resolution of 48 mm. The kernel of the median filter is set to be 3×1 to suppress non-realistic sudden changes of strain along the length. It should be noted that there is deterioration on the system spatial resolution due to the use of the median filter. The deterioration can be quantified through the expression $[W+(k-1)\cdot step]\cdot\Delta z$, where $k=3$ is the kernel size. Thus, the extent of deterioration is 57.6 mm, which is slightly greater than the 48-mm spatial resolution of the OFDR system. The additionally processed distributed strain sensing results for all three fibers are presented in Fig. 7.

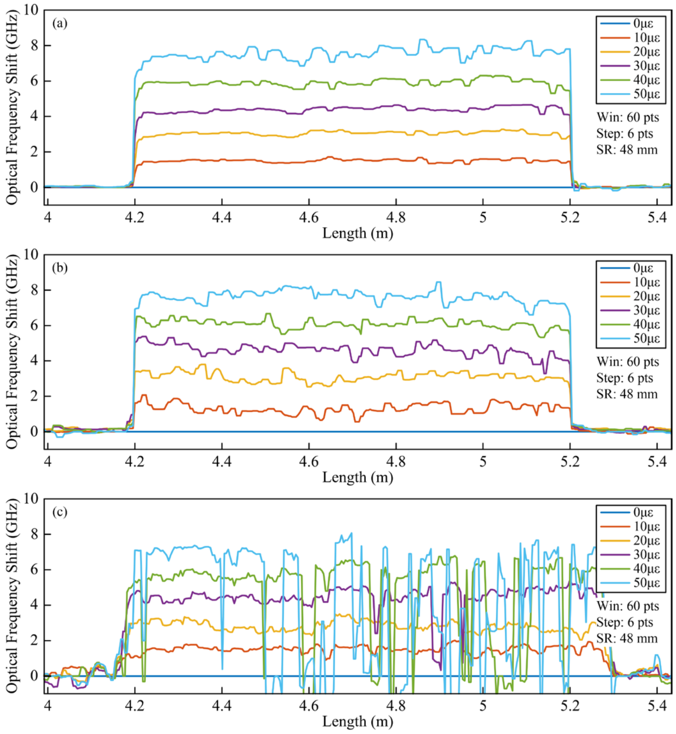

Fig. 7. Distributed strain sensing results by using the overlapping division method and median filtering with a window of 60 data points, a step size of 6 data points, and a spatial resolution of 48 mm: (a) Rayleigh enhanced sensing fiber; (b) OFS fiber; (c) standard single mode fiber.

When comparing the initial processing scheme captured in Fig. 4(a) with the improved processing scheme depicted in Fig. 7(a) for the Rayleigh enhanced fiber, the spatial resolution value is decreased by 45% while maintaining good sensing efficacy. Fig. 7(b) shows that the OFS fiber response is also improved. The median filtering algorithm removes the incorrect strain changes at the ends of the sensing segment, but shows significant fluctuations on the strain sensing curves. In the meantime, Fig. 7(c) indicates that the standard telecom single mode fiber is still incapable of detecting minor strain changes with the 48-mm spatial resolution. With the overlapping sliding window and the denoising algorithm, the standard telecom fiber required at least 100 data points (80-mm spatial resolution) with a step size of 10 data points to achieve effective strain measurements.

Due to the incapability of the standard single mode fiber with the 48-mm spatial resolution, the RMSE for optical frequency shifts and corresponding strain measurement resolution at each strain level shown in Fig. 7 are investigated for the Rayleigh enhanced sensing fiber and the OFS fiber only. These results are presented in Fig. 8(a). The denoising algorithm produced significant improvements for both test fibers. For the OFS sensing fiber, the RMSE at 50 με reduces from 33.58 με to 4.88 με. For the sensing fiber fabricated by the fs laser, the RMSE noise at 50 με reduces by as much as 89% from 26.31 με to 2.64 με. This should not be a surprise, given the backscattering signal from the fs enhanced sensing fiber is much stronger than that yielded by the OFS sensing fiber.

Results presented in Fig. 8(a) suggests that even 60 data points from OFDR measurements contains sufficient information for resolving the strain change, which can be unmasked by an effective denoising algorithm. An interesting question thus arises from Fig. 8(a) on how effective is Rayleigh backscattering signal enhancement to improve the OFDR measurements. This question is studied in Fig. 8(b).

The 1-m long fs laser enhanced fiber and UV laser enhanced fiber are equally divided into four 0.25-m segments, respectively. The measurement RMSE value at 50 με would be calculated for each segment individually instead of for the entire 1-m length. The first segment of the fs-enhanced fiber produces ~40-dB stronger backscattering signal than that of a standard single mode fiber, while the fourth segment only produces ~20-dB stronger backscattering signal. Fig. 8(b) compares RMSE results from the first segment through the fourth of the fs-enhanced sensing fiber and the UV-enhanced OFS fiber. The latter produces a constant ~10-dB stronger backscattering signal than that of standard fibers.

The RMSE values for the fs fiber segments show an upward trend. The first fs fiber segment with a ~40-dB backscattering enhancement achieves the best RMSE result of 0.37 GHz or 2.45 με at 50-με level. The fourth fs fiber segment with a ~20-dB backscattering signal enhancement yields a RMSE of 0.48 GHz or 3.18 με. In terms of the OFS fiber, the RMSE values remain relatively stable. The best RSME of the measurements is 0.71 GHz or 4.71 με at the first segment, while the worst is 0.75 GHz or 4.98 με at the fourth segment. Results presented in Fig. 8(b) indicate that once an effective denoising algorithm is used to remove noise from OFDR measurements, stronger backscattering signal (~40-dB enhancement) only yields limited improvements in sensing performance at the expense of excessive optical loss and sacrifice of interrogation length.

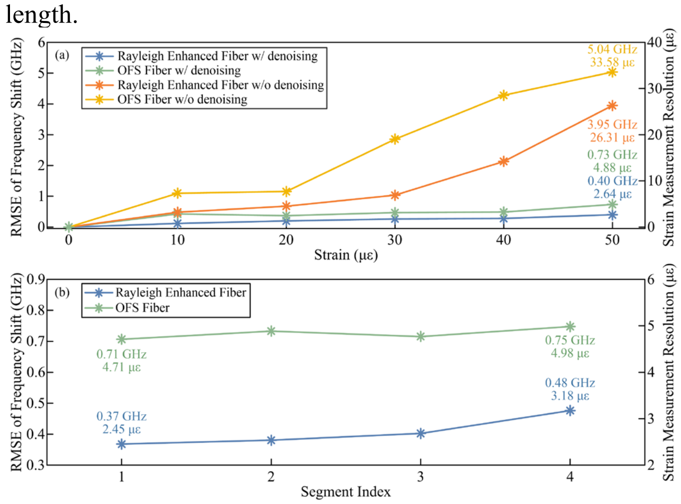

Fig. 8. RMSE of optical frequency shifts and strain measurement resolutions for two test fibers with 48-mm spatial resolution: (a) results for the 1-m Rayleigh enhanced fiber and the 1-m OFS fiber before and after using denoising algorithm; (b) results for four segments of the Rayleigh enhanced fiber and OFS fiber with denoising algorithm at 50 με.

IV. Conclusion and Discussion

Applications in distributed fiber optic sensing require vastly different interrogation techniques, data processing approaches, and sensing fiber specifications. Cost reductions of interrogator systems will enable a wider range of applications and end-uses of distributed fiber sensing techniques. Results presented in this paper show that the use of sensing fibers with enhanced backscattering profiles have the potential to reduce instrumentation costs of the OFDR system. As telecom distributed feedback (DFB) lasers are readily available at far lower cost than that of dedicated tunable lasers currently used for the OFDR system, this paper shows it is indeed possible to leverage the cost advantage of telecom DFB laser to expand applicability of OFDR-based distributed sensing.

Quantitative comparison between sensing fibers fabricated by fs lasers and that produced by UV lasers shows that OFDR performance improvements do not scale with the backscattering signal enhancement. Once an effective denoising algorithm removes system noise, further enhancement of backscattering signal of sensing fibers only yields limited improvements in sensor performance. Studies discussed in this paper will be useful in designing low-cost OFDR-based fiber sensors and gauging their performance.

Acknowledgment and Disclaimer

This work was performed under the support of the Department of Energy through Office of Nuclear Energy's grants DE-NE0008686 and DE-NE0008994. This work was also supported by the Department of Energy, National Energy Technology Laboratory, an agency of the United States Government, through a support contract with Leidos Research Support Team (LRST). Neither the United States Government nor any agency thereof, nor any of their employees, nor LRST, nor any of their employees, makes any warrant, expressed or implied, or assumes any legal liability or responsibility for the accuracy, completeness, or usefulness of any information, apparatus, product, or process disclosed, or represents that its use would not infringe privately owned rights. Reference herein to any specific commercial product, process, or service by trade name, trademark, manufacturer, or otherwise, does not necessarily constitute or imply its endorsement, recommendation, or favoring by the United States Government or any agency thereof. The views and opinions of authors expressed herein do not necessarily state or reflect those of the United States Government or any agency thereof.

References

[1] M. Badar, P. Lu, Q. Wang, T. Boyer, K. P. Chen, and P. Ohodnicki, "Real-time optical fiber-based distributed temperature monitoring of insulation oil-immersed commercial distribution power transformer," *IEEE Sens. J.*, vol. 21, no. 3, pp. 3013–3019, Feb. 2021.

[2] Q. Wang, K. Zhao, M. Badar, P. Lu, J. Zhao, and Y. Li *et al.*, "Low-cost OFDR distributed fiber sensing enabled by fiber with enhanced Rayleigh backscattering," *2021 Conference on Lasers and Electro-Optics (CLEO)*, paper ATh2S.7, 2021.

[3] Z. Sha, H. Feng, X. Rui, and Z. Zeng, "PIG tracking utilizing fiber optic distributed vibration sensor and YOLO," *J. Lightwave Technol.*, vol. 39, no. 13, pp. 4535–4541, Jul. 2021.

[4] M. Badar, P. Lu, M. Wang, Q. Wang, K. P. Chen, and M. Buric *et al.*, "Integrated auxiliary interferometer to correct non-linear tuning errors in OFDR," in *Proc. SPIE 11405*, 2020.

[5] Luna Innovations, "OBR 4600 optical backscatter reflectometer," OBR 4600 datasheet, Feb. 2019.

[6] Z. Wang, L. Zhang, S. Wang, N. Xue, F. Peng, and M. Fan *et al.*, "Coherent Φ-OTDR based on I/Q demodulation and homodyne detection," *Opt. Express*, vol. 24, no. 2, pp. 853–858, Jan. 2016.

[7] N. Lalam, P. S. Westbrook, J. Li, P. Lu, and M. P. Buric, "Phase-sensitive optical time domain reflectometry with Rayleigh enhanced optical fiber," *IEEE Access*, vol. 9, pp. 114428–114434, Aug. 2021.

[8] S. Loranger, M. Gagné, V. Lambin-lezzi, and R. Kashyap, "Rayleigh scatter based order of magnitude increase in distributed temperature and strain sensing by simple UV exposure of optical fibre," *Sci. Rep.*, vol. 5, art. no. 11777, Jun. 2015.

[9] M. Wang, K. Zhao, S. Huang, J. Wu, P. Lu, and P. Ohodnicki *et al.*, "Reel-to-reel fabrication of in-fiber low-loss and high-temperature stable Rayleigh scattering centers for distributed sensing," *IEEE Sens. J.*, vol. 20, no. 19, pp. 11335–11341, Oct. 2020.

[10] L. Zhang, Z. Yang, N. Gorbatov, R. Davidi, M. Galal, and L. Thevenaz *et al.*, "Distributed and dynamic strain sensing with high spatial resolution and large measurable strain range," *Opt. Lett.*, vol. 45, no. 18, pp. 5020–5023, Sep. 2020.

[11] K. Naeem, Y. Kwon, Y. Chung and I. Kwon, "Bend-loss-free distributed sensor based on Rayleigh backscattering in Ge-doped-core PCF," *IEEE Sens. J.*, vol. 18, no. 5, pp. 1903–1910, Mar. 2018.

[12] A. Beisenova, A. Issatayeva, S. Sovetov, S. Korganbayev, M. Jelbuldina, and Z. Ashikbayeva *et al.*, "Multi-fiber distributed thermal profiling of minimally invasive thermal ablation with scattering-level multiplexing in MgO-doped fibers," *Biomed. Opt. Express*, vol. 10, no. 3, pp. 1282–1296, Mar. 2019.

[13] V. Fuertes, N. Grégoire, P. Labranche, S. Gagnon, R. Wang, and Y. Ledemi *et al.*, "Engineering nanoparticle features to tune Rayleigh scattering in nanoparticles-doped optical fibers," *Sci. Rep.*, vol. 11, art. no. 9116, Apr. 2021.

[14] D. Tosi, C. Molardi, M. Sypabekova, and W. Blanc, "Enhanced backscattering optical fiber distributed sensors: tutorial and review," *IEEE Sens. J.*, vol. 21, no. 11, pp. 12667–12678, Jun. 2021.

[15] Z. Lu, T. Robine, C. Molardi, F. Pigeonneau, D. Tosi, and W. Blanc, "Toward engineered nanoparticle-doped optical fibers for sensor applications," *Front. Sens.*, vol. 2, art. no. 805351, Feb. 2022.

[16] A. Yan, S. Huang, S. Li, R. Chen, P. Ohodnicki, and M. Buric *et al.*, "Distributed optical fiber sensors with ultrafast laser enhanced Rayleigh backscattering profiles for real-time monitoring of solid oxide fuel cell operations," *Sci. Rep.*, vol. 7, art. no. 9360, Aug. 2017.

[17] T. J. Ahn, J. Y. Lee, and D. Y. Kim, "Suppression of nonlinear frequency sweep in an optical frequency-domain reflectometer by use of Hilbert transformation," *Appl. Opt.*, vol. 44, no. 35, pp. 7630–7634, Dec. 2005.

[18] U. Glombitza and E. Brinkmeyer, "Coherent frequency-domain reflectometry for characterization of single-mode integrated optical waveguides," *J. Lightwave Technol.*, vol. 11, no. 8, pp. 1377–1384, Aug. 1993.

[19] J. Cui, S. Zhao, D. Yang, and Z. Ding, "Investigation of the interpolation method to improve the distributed strain measurement accuracy in optical frequency domain reflectometry systems," *Appl. Opt.*, vol. 57, no. 6, pp. 1424–1431, Feb. 2018.

[20] M. Froggatt and J. Moore, "High-spatial-resolution distributed strain measurement in optical fiber with Rayleigh scatter," *Appl. Opt.*, vol. 37, no. 10, pp. 1735–1740, Apr. 1998.

[21] M. A. Soto, J. A. Ramírez, and L. Thévenaz, "Reaching millikelvin resolution in Raman distributed temperature sensing using image processing," in *Proc. SPIE 9916*, 2016.

[22] M. A. Soto, Z. Yang, J. A. Ramírez, S. Zaslawski, and L. Thévenaz, "Evaluating measurement uncertainty in Brillouin distributed optical fibre sensors using image denoising," *Nat. Commun.*, vol. 12, art. no. 4901, Aug. 2021.

[23] I. Pitas and A. N. Venetsanopoulos, "Order statistics in digital image processing," in *Proc. IEEE*, vol. 80, no. 12, pp. 1893–1921, Dec. 1992.

[24] S. Zhao, J. Cui, Z. Wu, and J. Tan, "Accuracy improvement in OFDR-based distributed sensing system by image processing," *Opt. Laser. Eng.*, vol. 124, 105824, Jan. 2020.

[25] J. P. von der Weid, R. Passy, G. Mussi, and N. Gisin, "On the characterization of optical fiber network components with optical frequency domain reflectometry," *J. Lightwave Technol.*, vol. 15, no. 7, pp. 1131–1141, July 1997.

Qirui Wang received the B.S. degree in mechanical engineering and automation from Beijing University of Technology, Beijing, China, in 2015, and the M.S. degree in instrumentation science and technology from Beihang University, Beijing, China, in 2018. He is currently working toward the Ph.D. degree in electrical and computer engineering at the University of Pittsburgh.

His research interests include distributed optical fiber sensing and machine learning.

Kehao Zhao received the B.S. degree in mechanical engineering and automation from Beijing University of Posts and Telecommunications, Beijing, China, in 2016, and the M.S. degree in mechanical engineering from the University of Pittsburgh, Pittsburgh, PA, USA, in 2019. He is currently working toward the Ph.D. degree with Electrical and Computer Engineering Department, University of Pittsburgh.

His research interests include the study of optical fiber sensors.

Mudabbir Badar received the Ph.D. degree from Kochi University of Technology, Japan, in 2016. His area of expertise is in optical fiber sensing and imaging. At the time of conception of this paper, he was working as a Postdoctoral Researcher at the National Energy Technology Laboratory.

Xinruo Yi received the B.S. degree in composites materials and engineering from Northwestern Polytechnical University in 2015, and the M.S. degree in material science and engineering from the University of Florida in 2017. She is currently pursuing the Ph.D. degree in electrical and computer engineering with the University of Pittsburgh.

Her current research interest includes fiber optical sensor fabrication and development.

Ping Lu (M'13) is currently working as a development engineer at OFS Fitel, LLC, Avon, CT, USA. His research interests include specialty optical fiber and fiber-optic sensing system development for a wide range of energy and infrastructure asset monitoring applications.

Michael Buric is a research scientist at the National Energy Technology Laboratory in Morgantown, West Virginia in the Lab's Research and Innovation Center on the Functional Materials Development Team. His current research interests include the modeling and fabrication of fiber-based optical sensors and devices, harsh-environment sensing for energy applications, laser-heated pedestal growth of single-crystal optical fibers, novel waveguide fabrication, distributed sensing, fiber embedding, additive manufacturing, and applications of Raman spectroscopy. He has been awarded several patents and has published extensively in the proceedings of the SPIE and elsewhere. He was a recipient of SPIE's 2017 Rising Researcher Award and a 2020 Carnegie Science Center Innovation Award in Energy. He is also the lead Laser Safety Officer at NETL in addition to overseeing several energy-related research projects.

Zhi-Hong Mao (S'96–M'05–SM'09) received the dual Bachelor's degrees in automatic control and applied mathematics and the M.Eng. degree in intelligent control and pattern recognition from Tsinghua University, Beijing, China, in 1995 and 1998, respectively, the S.M. degree in aeronautics and astronautics from Massachusetts Institute of Technology, Cambridge, MA, USA, in 2000, and the Ph.D. degree in medical engineering and medical physics from the Harvard-MIT Division of Health Sciences and Technology, Cambridge, in 2006.

He joined the University of Pittsburgh, Pittsburgh, PA, USA, as an Assistant Professor in 2005 and became a Professor in 2018.

Kevin P. Chen graduated from Xiamen University, Xiamen, China, in 1994 with the dual B.S. degrees in control science and physics. He joined Pittsburgh after completing the Ph.D. training with the University of Toronto, Toronto, ON, Canada, in 2002.

He is the Paul E. Lego Chair Professor of engineering with the University of Pittsburgh, Pittsburgh, PA, USA. He performed research in fiber optics, integrated optics, and laser manufacturing. He is the co-inventor of 15 US patents and co-author of more than 250 technical papers.